Precipitation fuels dissolved greenhouse gas (CO$_2$, CH$_4$, N$_2$O) dynamics in a peatland-dominated headwater stream: results from a continuous monitoring setup

David R. Piatka*, Raphaela L. Nánási†, Ricky M. Mwanake, Florian Engelsberger, Georg Willibald, Frank Neidl and Ralf Kiese

Karlsruhe Institute of Technology, Institute for Meteorology and Climate Research, Atmospheric Environmental Research (IMK-IFU), Garmisch-Partenkirchen, Germany

Stream ecosystems are actively involved in the biogeochemical cycling of carbon (C) and nitrogen (N) from terrestrial and aquatic sources. Streams hydrologically connected to peatland soils are suggested to receive significant quantities of particulate, dissolved, and gaseous C and N species, which directly enhance losses of greenhouse gases (GHGs), i.e., carbon dioxide (CO$_2$), methane (CH$_4$), and nitrous oxide (N$_2$O), and fuel in-stream GHG production. However, riverine GHG concentrations and emissions are highly dynamic due to temporally and spatially variable hydrological, meteorological, and biogeochemical conditions. In this study, we present a complete GHG monitoring system in a peatland stream, which can continuously measure dissolved GHG concentrations and allows to infer gaseous fluxes between the stream and the atmosphere and discuss the results from March 31 to August 25 at variable hydrological conditions during a cool spring and warm summer period. Stream water was continuously pumped into a water-air equilibration chamber, with the equilibrated and actively dried gas phase being measured with two GHG analyzers for CO$_2$ and N$_2$O and CH$_4$ based on Off-Axis Integrated Cavity Output Spectroscopy (OA-ICOS) and Non-Dispersive Infra-Red (NDIR) spectroscopy, respectively. GHG measurements were performed continuously with only shorter measurement interruptions, mostly following a regular maintenance program. The results showed strong dynamics of GHGs with hourly mean concentrations up to 9959.1, 1478.6, and 9.9 parts per million (ppm) and emissions up to 313.89, 1.17, and 0.40 mg C or N m^{-2}h^{-1} for CO$_2$, CH$_4$, and N$_2$O, respectively. Significantly higher GHG concentrations and emissions were observed shortly after intense precipitation events at increasing stream water levels, contributing 59% to the total GHG budget of 762.2 g m^{-2} CO$_2$-equivalents (CO$_2$-eq). The GHG data indicated a constantly strong terrestrial signal from peatland pore waters, with high concentrations of dissolved GHGs being flushed into the stream water after precipitation. During drier periods, CO$_2$ and CH$_4$ dynamics were strongly influenced by in-stream metabolism. Continuous and high-frequency GHG data are needed to assess short- and long-term dynamics in stream ecosystems and for improved source partitioning between *in-situ* and *ex-situ* production.

KEYWORDS

streams, peatlands, global warming, greenhouse gases, CO$_2$, CH$_4$, N$_2$O, continuous monitoring

1 Introduction

Streams and rivers receive and transport large amounts of terrestrial and riverine dissolved and particulate carbon (C) and nitrogen (N) and are hotspots for biogeochemical turnover processes (Downing et al., 2012; Raymond et al., 2013; Piatka, 2022; Battin et al., 2023). Due to their close connectivity to the surrounding environment, including other subsurface and surface water bodies such as ponds, lakes, reservoirs, estuaries, hyporheic zones (HZs; mixing zones of stream water and groundwater), and groundwaters, lotic ecosystems act as integrators of entire catchments (Allan, 2004; Webb et al., 2019; Piatka et al., 2021). Therefore, their C and N cycles react sensitively to pollution, hydrology, climate, and land use changes (Song et al., 2018; Piatka et al., 2022a; Mwanake et al., 2023; Upadhyay et al., 2023). Recent estimations have highlighted the significance of lotic ecosystems as emitters of the most important greenhouse gases (GHGs): carbon dioxide (CO_2), methane (CH_4), and nitrous oxide (N_2O) (Battin et al., 2009; Raymond et al., 2013; Hotchkiss et al., 2015; Marzadri et al., 2021; Mwanake et al., 2022). Despite lower daily fluxes compared to CO_2, CH_4, and N_2O can significantly contribute to overall GHG balances from fluvial ecosystems due to their higher global warming potentials (GWPs) of 27.2 (non-fossil origin) and 273, respectively, referenced to CO_2 on a 100-year time scale (Intergovernmental Panel on Climate Change, 2021).

According to the Paris Agreement in 2015, substantial efforts should be taken to limit global warming to 1.5°C above pre-industrial levels (Tollefson and Weiss, 2015; Intergovernmental Panel on Climate, 2022). A critical component of this goal might include conservation activities of pristine and restoration efforts of degraded and drained peatlands with their functions as large C pools and net GHG sinks (Drösler et al., 2008; Höper et al., 2008; Harenda et al., 2018; Alexandrov et al., 2020). Here, availabilities of oxygen (O_2) or other terminal electron acceptors (e.g., SO_4^{2-}, NO_3^-, Mn^{4+}, and Fe^{3+}) in peatland soils act as essential drivers of produced GHGs (Blodau, 2011; Bridgham et al., 2013; Lyu et al., 2018). Well-aerated and oxygenated peatland soils (e.g., drained and managed peatlands) are significant sources of CO_2 by aerobic respiration, whereas N_2O is mainly produced by nitrification and denitrification processes at variable oxygen levels (Kasimir-Klemedtsson et al., 1997; Maljanen et al., 2010; Frolking et al., 2011; Butterbach-Bahl et al., 2013; Liu et al., 2020). Under water-logged and anoxic conditions (e.g., pristine and re-wetted peatlands), CH_4 is mainly produced by methanogens if other terminal electron acceptors are depleted, and oxygenated carbon compounds (e.g., CO_2) are available (Lyu et al., 2018; Gao et al., 2019). At anoxic to oxic interfaces, methanotrophic microbes can oxygenize CH_4 to produce energy and CO_2 (Hanson and Hanson, 1996; Hornibrook et al., 2009). These basic concepts of GHG production are also valid in aquatic ecosystems.

In recent decades, increasing attention has been attributed to lateral losses of dissolved, particulate, and gaseous C and N species from peatland soils to hydrologically connected ditch and headwater stream systems in peatland-dominated catchments (Hope et al., 2001; Julian et al., 2004; Dinsmore et al., 2010; Billett and Harvey, 2013; Evans et al., 2015; Campeau et al., 2017; Taillardat et al., 2022). Peatland streams have been found

to be highly supersaturated with dissolved CO_2, CH_4, and N_2O and rich in dissolved and particulate organic C (DOC, POC) and N (DON, PON) as a result of *ex-situ* sources, e.g., surface water run-off and pore water seepage from the surrounding environment, or *in-situ* production (Hope et al., 2001; Billett and Moore, 2008; Dinsmore et al., 2010; Taillardat et al., 2022). Mainly during and after intense precipitation events (flushing effects), large quantities of peatland soil GHGs can be mobilized to the stream network, whereas washed-in organic matter can further fuel in-stream GHG production (Billett et al., 2004; Dinsmore and Billett, 2008; Raymond et al., 2016; Jennings et al., 2020). Magnitudes of respective riverine GHG evasions to the atmosphere can show a high temporal and spatial variability on diel to seasonal scales with gas-specific solubilities, partial gas pressure differences between the atmosphere and stream water, and gas exchange velocities (k) as the most critical drivers (Bade, 2009; Raymond et al., 2012; Hall Jr and Ulseth, 2020; Attermeyer et al., 2021). Different experimental and modeling approaches were performed to measure and asses variable k values of varying stream systems as a significant parameter for GHG emissions, however, with their own temporal and spatial limitations and uncertainties (Raymond et al., 2012; Berg and Pace, 2017; Appling et al., 2018; Hall Jr and Ulseth, 2020).

Most studies directly investigating aquatic GHG losses from peatland-dominated streams have focused on selected GHGs in the C cycle, i.e., CO_2 and CH_4 (Hope et al., 2001; Billett and Moore, 2008; Dinsmore and Billett, 2008; Wallin et al., 2010; Vermaat et al., 2011; Evans et al., 2015; Campeau et al., 2017; Taillardat et al., 2022). Only a few studies have simultaneously measured CO_2, CH_4, and N_2O to enable a complete GHG balance; however, all measurements were performed as discrete samples (Dinsmore, 2008; Dinsmore et al., 2010, 2013; Aho and Raymond, 2019). Based on our current knowledge, no study has carried out continuous and simultaneous measurements of all GHGs. However, considering the possible importance of short-term GHG emission peaks, e.g., during rainfall events, for the overall net GHG balance of peatlands and peatland-associated streams and their potential relevance to counteract climate change, only continuous data can provide sufficient resolution. Ongoing advancements in laser spectroscopy coupled to air-water equilibration systems can be used to measure selected or even all three GHGs with high temporal resolution and accuracy (Gülzow et al., 2011; Santos et al., 2012; Gonzalez-Valencia et al., 2014; Webb et al., 2016).

This work describes a system for continuous and long-term GHG concentration measurements and relevant environmental parameters in a peatland-dominated headwater stream, including details on all devices, performed maintenance works, measurement stability, and possible limitations. With this setup, we aimed to

1) Adapt and test technical and personnel efforts as well as the long-term stability of continuous GHG concentration measurements using laser spectroscopy coupled to an air-water equilibration unit.
2) Share technical details and experiences with the aquatic research community.
3) Demonstrate the potential of continuous multi-species measurements for improved understanding of variable GHG (i.e., CO_2, CH_4, N_2O) concentrations, inferred emissions and

budgets, and interactions with environmental controls and changes in stream water levels.

After describing the study site, overall setup, and measurement performance, an almost 5-month dataset from March 31 to August 25, 2023, is presented and briefly discussed.

2 Study location and measurement setup

2.1 Observation site

The observation site Haselbach (HAS) (latitude, longitude, altitude above sea level (asl): 47.794806, 11.4267, 591.3 m), a headwater stream originating at the confluence of the headwater streams Holmbach and Auer Bach further south, is located on the property of the foundation "Kunst und Natur"[1] in the pre-alpine region approximately 50 km south of the city Munich in Bavaria, Germany (see Figure 1A). The stream channel has an average depth of 0.96 m and width of 2.20 m with low flow velocities due to a generally low downward slope of the stream channel (0.1546%) (Planungsbüro U-Plan, 2016). The stream is located at the lower part of the Haselbach catchment with a total size of 7.84 km^2 (Figure 1B) and drains a peatland-dominated landscape with partly re-wetted areas (Figure 2). The selected study location lies approximately 500 m downstream of an adjacent re-wetted peatland and an extensively grazed grassland.

In general, the climate in this region can be classified as humid and temperate based on the closest ($\sim$10 km distance) weather station, Attenkam (47.877428, 11.364282, 670 m), from the German Weather Service (DWD), with an annual mean precipitation and air temperature of 1,140.6 mm and 8.6°C, respectively, for the period 1991 and 2020. Most precipitation occurs as rainfall in the warmer months between May and September (58.5%) (Deutscher Wetterdienst, 2023).

The landscape and geology (Figure 2) in the area of the observation site were primarily influenced by the former ice age of Würm, which lasted until $\sim$10,000 years ago. After the ice age, a former meltwater lake in the so-called Wolfratshausener basin deposited lake sediments with high proportions of clay minerals associated with low water permeability characteristics (Jerz, 1979). The combination of the geological and hydrological settings with high amounts of meltwater from the retreating glaciers and a generally humid and temperate climate in this region have favored the formation of multiple fens, bogs, and transitional bogs (Kaule and Peringer, 2015). Peat soils (55.3%) are the most dominant soil type within the catchment, which can be differentiated by bog (26.8%), fen (17.8%), and transitional bog peat (10.7%) (Figure 2) (Bayerisches Landesamt für Umwelt, 2023). To sustain increasing energy and food demands, peatlands, as in the study region, have been intensively used for peat mining and drained for grassland and forest land use since the 19th century[2] (Bernrieder, 2003). Today, a

significant fraction of these peatland systems can be considered as degraded (>95% in Germany) (Joosten et al., 2017).

2.2 General setup

2.2.1 Energy trailer and technical setup

An energy trailer was positioned $\sim$5 m next to the HAS stream to provide a permanent energy supply and remote control (Figure 3A) for long-term and continuous stream measurements (Figures 3B–E). Energy is supplied by two LiFePO$_4$ batteries (25.6 V−200 Ah, Victron Energy BV, the Netherlands) connected to an inverter (MultiPlus 24/5000/120-100, Victron Energy BV, the Netherlands). During the daytime, four solar panels charge the batteries (360 W, 24 V, peak total output of 1,440 W). In cases of increased power consumption or insufficient solar energy input, a diesel generator (AGT-DC 600-24 PVMV-N, Fischer Panda GmbH, Germany) with a maximum output of 6 kW charges the batteries when the charge level reaches 30% or less. The energy trailer provides plugs for 12 and 24 DC and 230 V AC output. Measuring devices were connected to the board grid with 12 and 24 V without losses via the inverter. Additional electrical appliances can be operated by installing multiple sockets. An air conditioner (5 kW, AC-M5W, Dantherm Group A/S, Denmark) was used to control indoor air temperatures. The whole trailer was made by GME Systems GmbH in cooperation with Hecka GmbH (both Germany).

A field laptop was installed for data storage and visualization. An industrial router provided Internet access with 4G LTE connectivity (TK815L-EXW, Welotec GmbH, Germany) for remote access to the laptop. Near real-time data transfer was performed via a synchronization software (NextCloud private, on premise).[3] A network camera (AXIS P5655-E PTZ, AXIS Communications GmbH, Germany) was also installed outside the energy trailer for surveillance and maintenance purposes (Figure 3A).

2.2.2 Continuous greenhouse gas (GHG) measurements

In the HAS stream, a bilge pump (Rule 24DA, Xylem Inc., USA) was installed about 10 cm above the stream bed to ensure permanent water coverage even at lower discharge conditions (Figure 3C). To avoid direct pumping of large particulate organic matter (POC), such as water plant remains, a perforated metal plate was installed $\sim$1 m upstream. The pump was placed inside a perforated metal cage encased in a coarse plastic mesh grid, followed by a larger perforated metal cage. This configuration shielded the pump from direct large POC suction and served as a course particle filter. Stream water was continuously pumped through a hose (inner diameter of 12.7 mm) into a commercially available water-air equilibration chamber (Rad Aqua, DURRIDGE Company, Inc., USA) through two spay nozzles with a flow rate of 4.1 L min^{-1} at 138 Pa water pressure (Figures 3D, 4). A manufactured Plexiglas disc was placed on top to reduce the gas exchanges of the collected water in the tray at the bottom

---

1   https://kunst-und-natur.de/ (accessed August 21, 2023).

2   https://kunst-und-natur.de/nantesbuch/gelaende (accessed August 22, 2023)

3   https://nextcloud.com/ (accessed October 6, 2023).
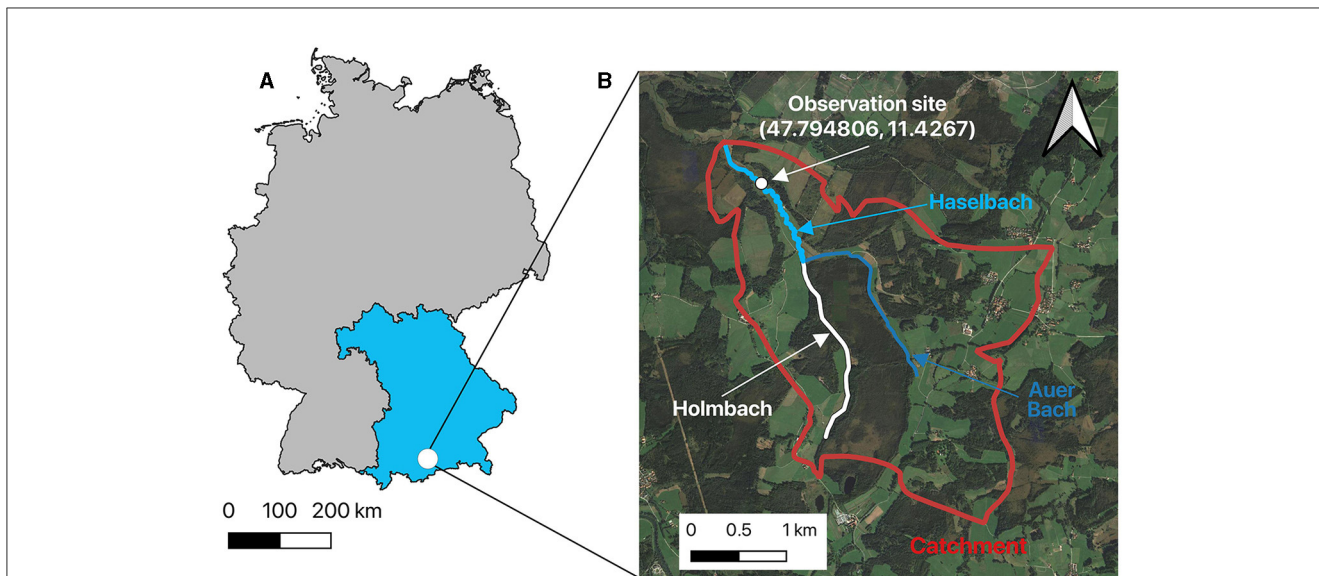
FIGURE 1
(A) General overview of the study location in Germany (gray) and Bavaria (blue) and **(B)** close-up view of the observation site (white circle) including coordinates (latitude, longitude) with the investigated stream Haselbach (light blue line), the up-stream tributaries Holmbach (gray line), and Auer Bach (dark blue line) in the catchment (red line) (basemap: ©2015 Google).
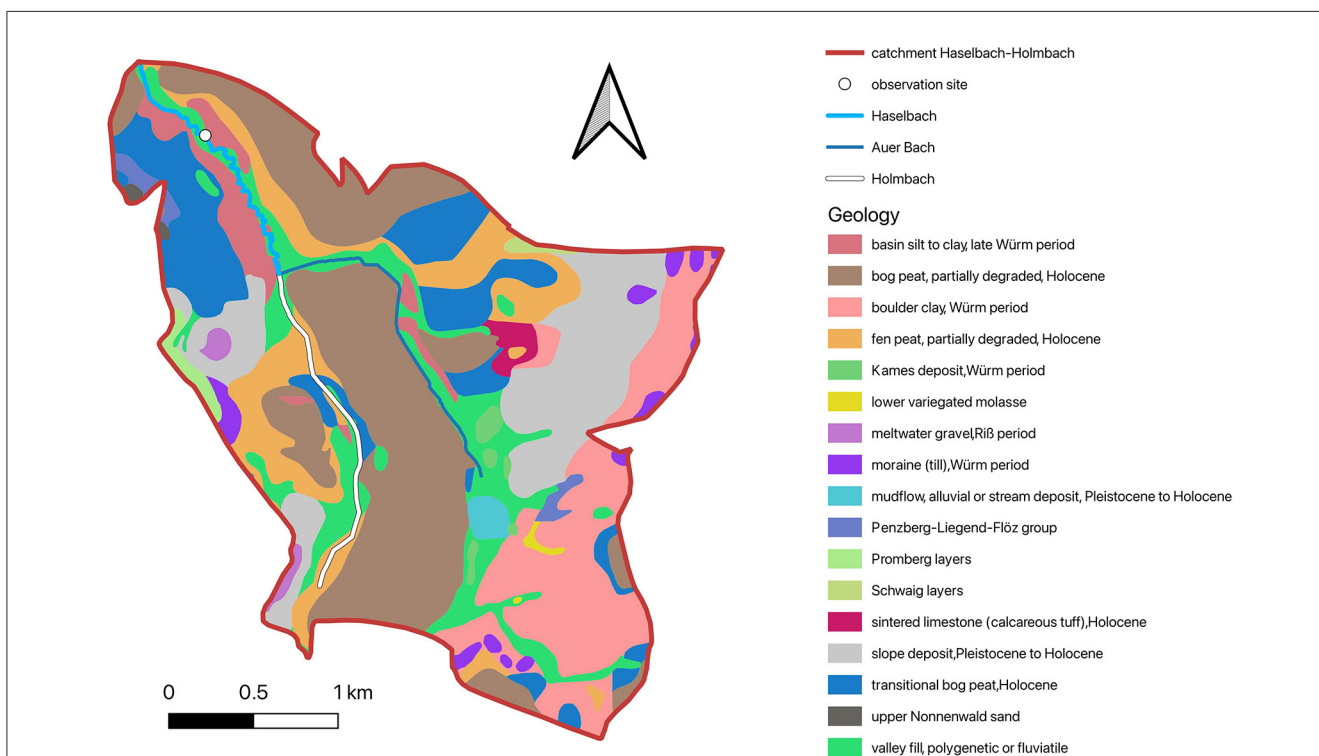
FIGURE 2
Overview of the investigated study site (white circle) in the stream Haselbach (light blue line) with further upstream tributaries Holmbach (white line) and Auer Bach (dark blue line) with classifications of the present geology in the catchment (data source: Bayerisches Landesamt für Umwelt, 2023).

with the atmosphere. A temperature sensor (Omega Temperature Probe, Omega Engineering Inc., USA) and logger (Omega OM-EL-USB-TC Temperature Logger, Omega Engineering Inc., USA) recorded chamber temperatures at 10-min intervals.

An active moisture exchanger with an internal pump and a Nafion membrane (DRYSTIK, ADS-3R, DURRIDGE Company,

Inc., USA) was used to dry the air sample stream, which was continuously drawn and pumped back into the chamber headspace of the water-air equilibrator in a closed loop (Figures 3E, 4). A flow rate of $1.5\,L\,min^{-1}$ was adjusted using the high airflow output valve of the DRYSTIK. A 3 m Teflon vent (inner diameter of 1.6 mm) was installed before the gas inlet to balance
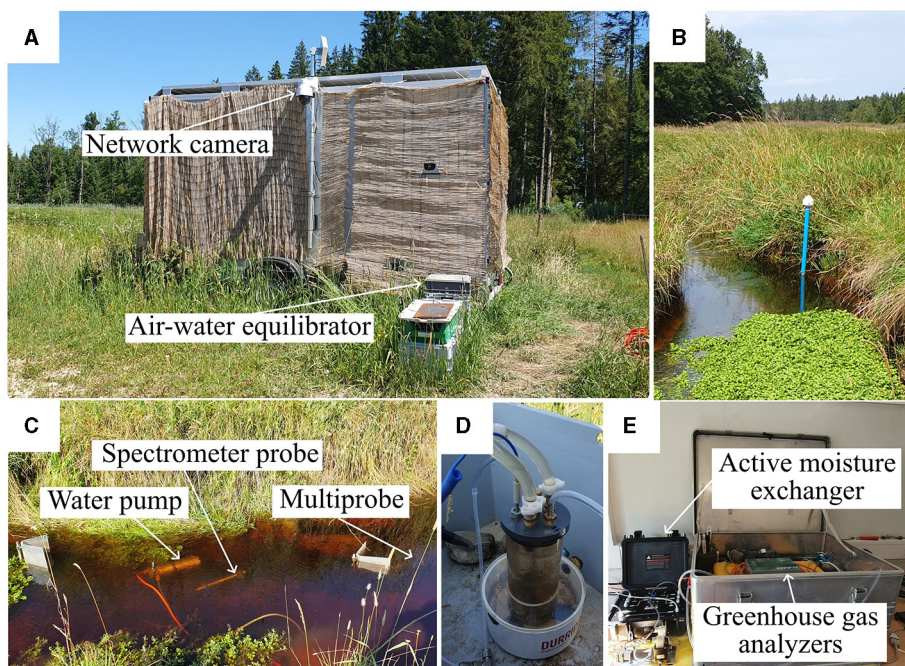
FIGURE 3
Overview of the measurement setup at the Haselbach stream with **(A)** the energy trailer including an outdoor network camera and an air-water equilibration system, **(B)** continuous water level measurements, **(C)** water pump and water chemistry probes, **(D)** a close-up view of air-water equilibrator, and **(E)** greenhouse gas (GHG) analyzers, i.e., CO_2, CH_4, and N_2O, attached to an active moisture exchanger inside the energy trailer.
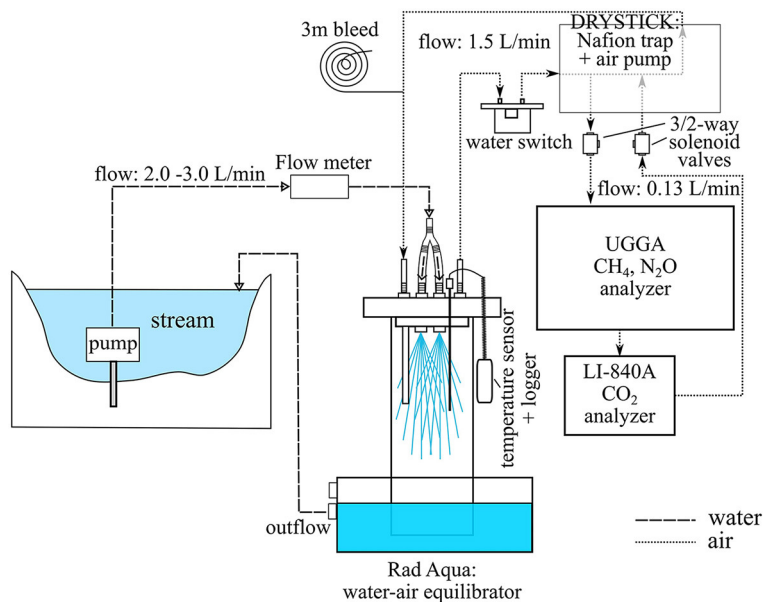
FIGURE 4
General overview of continuous dissolved greenhouse gas (GHG) measurements in the investigated Haselbach (HAS) stream. The setup includes water pumped to an air-water equilibrator with the desiccated (DRYSTICK) sample air subsequently being measured for CO_2 and CH_4, and N_2O concentrations using an Ultraportable Greenhouse Gas Analyzer (UGGA) based on Off-Axis Integrated Cavity Output Spectroscopy (OA-ICOS) and a LI-840A based on Non-Dispersive Infra-Red (NDIR) spectroscopy, respectively. The water switch and the 3/2-way solenoid valves prevented water from entering the DRYSTICK and GHG analyzers.

possible atmospheric pressure differences and prevent rising water levels within the equilibration chamber as recommended by the manufacturer. Flow rates through the vent air were checked with

a flow meter (Ellutia 7000 GC Flowmeter, Ellutia Ltd., UK) and showed negligible airflow in the 4–5-mL min^{-1} range. To prevent water suction into the DRYSTICK and GHG analyzers a water

switch (DURRIDGE Company, Inc., USA) was preconnected to the DRYSTIK as an emergency feature to cut the power supply, which worked in combination with two 3/2-way solenoid valves (Bürkert GmbH, Germany) between the DRYSTICK and the GHG analyzers (Figure 4). In case of an activated water switch, the valves opened to ambient air to maintain atmospheric pressure within the GHG analyzers.

A GHG analyzer for N_2O and CH_4 [Ultraportable Greenhouse Gas Analyzer (UGGA), N2OM1-919, Los Gatos Research (LGR), USA] with Off-Axis Integrated Cavity Output Spectroscopy (OA-ICOS) was put in sequence with a CO_2 gas analyzer (LI-840A, LI-COR Biosciences, USA) based on Non-Dispersive Infra-Red (NDIR). The internal pump of the UGGA pumped sample air in a closed loop out of the closed loop of the DRYSTIK setup (Figure 4) at an average flow rate of 0.13 L/min, which was measured with a flowmeter (red-y compact meter GCM, Vögtlin Instruments GmbH, Switzerland). GHG gas concentrations were measured per second with a measurement range of 0–10 ppm (± 0.4 ppb) and 0–100 ppm (± 2 ppb) for N_2O and CH_4, respectively, and 20,000 (± 1) ppm for CO_2. Only dry air mole fractions of CO_2, CH_4, and N_2O are reported in this study. Measurement data of the UGGA were stored on an instrument internal computer with data storage capacities suitable for long-term measurements and visualized on the field laptop via a VNC Viewer (RealVNC, version 7.6.0).[4] The appropriate LI-COR software [LI-840A Instrument (Embedded) Software, version 2.1.0][5] was used to store and visualize the LI-840A data on the field laptop.

2.2.3 Additional stream and water quality parameters

Continuous water level measurements (April 6 to May 26 hourly, then in 10-min intervals) were performed to capture the variability of discharge conditions of the HAS stream. A slotted groundwater pipe (2 inches, PVC-U, DN50, DIN 4925) with a length of 1 m and a slit width of 0.5 mm was partially inserted into the stream bed at the deepest part of the water profile with lowered flow velocities. A data logger (OTT ecoLog 1000, OTT HydroMet GmbH, Germany) for atmospheric pressure-corrected water levels and temperatures was inserted into a second solid pipe attached on top. Communication and data access were enabled via a password-protected Bluetooth Low Energy (BLE) interface and a modem (HL 7800-M Global) for long-distance data transfer based on Internet of Things (IoT) LTE-M (CAT M1) technology. A weatherproof and lockable top cap (OTT ecoCap, OTT HydroMet GmbH, Germany) protected the data logger and antenna, maintaining communication functionalities.

A magnetic-inductive flow meter (OTT MFpro, OTT HydroMet GmbH, Germany) was used for discrete mean water flow velocity measurements at different hydrologic conditions. Correlations with sporadic measured water levels covering low to high stream water levels allowed continuous flow velocity estimations. A detailed overview of respective measurement

---

4   https://www.realvnc.com/de/ (accessed August 29, 2023).

5   https://www.licor.com/env/support/LI-840A/software.html   (accessed August 29, 2023).

FIGURE 5
Linear correlation (y = 0.8005x−0.3191) between measured stream velocities and respective water levels.
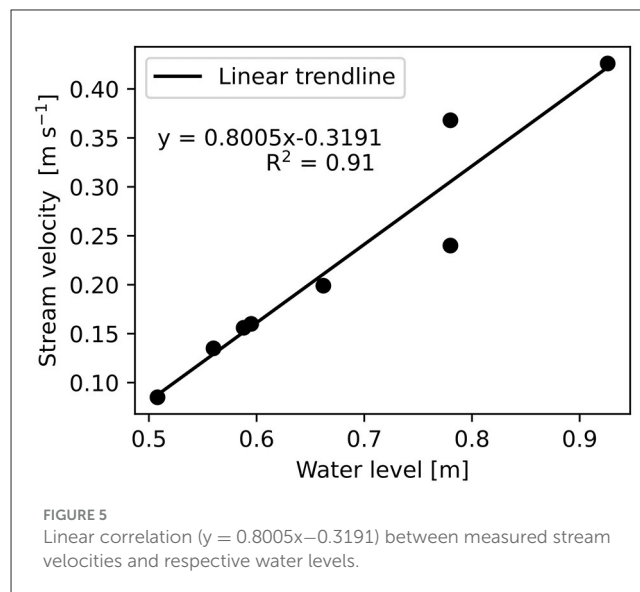
TABLE 1   Measurements of flow velocities and mean water depths at variable water levels.

Date	Velocity [m s^{-1}]	Mean depth[m]	Water level [m]
2023-04-06	0.085	0.347	0.508
2023-04-13	0.426	0.715	0.926
2023-04-14	0.24	0.539	0.78
2023-04-17	0.199	0.483	0.662
2023-04-20	0.368	0.56	0.78
2023-04-21	0.16	0.422	0.595
2023-04-24	0.156	0.393	0.588
2023-04-25	0.135	0.389	0.56

results and corresponding water levels is presented in Table 1. Discrete water levels and Vs ranged between 0.508 and 0.926 m and 0.085 and 0.426 m s^{-1}, respectively. A significant positive linear relationship (coefficient of determination (R^2) = 0.91, $p < 0.05$) between these parameters could be observed (Figure 5), which was used to estimate Vs from continuous water level data.

Most crucial chemical and physical water parameters were recorded in 10-min temporal (hourly before May 26) resolution with a Pro DSS multiprobe (YSI Inc., USA) and Spectrometer Probe V3 (spectro::lyser V3, s::can GmbH, Austria) approximately 10 cm above the stream bed to ensure continuous monitoring even at lower water levels. A summary of applied devices for stream and water quality parameters, including measurement ranges and precisions, is shown in Table 2.

2.3 Data processing and greenhouse gas (GHG) flux and balance calculations

Data from GHG analyzers, water level loggers, and water chemistry probes were collected weekly on a USB flash drive. Incorrect measurement data during and shortly after maintenance

TABLE 2 Overview of all site parameters and used devices for stream and water quality parameter measurements with measurement ranges and precisions.

Probe	Water parameter, abbreviation	Unit	Measurement range	Accuracy
Pro DSS multiprobe	temperature, T	°C	−5–70	±0.2
	pH	-	0–14	±0.2
	Dissolved oxygen, DO	mg L^{-1}; %	0–200	±2%
	Specific conductance, SPC	µS cm^{-1}	0–100	±2%
Spectro::lyser V3 (OPL = 5 mm)	dissolved organic carbon, DOC	mg L^{-1}	0–180	±4%
	Total organic carbon, TOC	mg L^{-1}	0–210	±4%
	Total suspended solids, TSS	mg L^{-1}	0–1,200	n.a.
	Turbidity	FTU/NTU	0–1,400	n.a.
	Nitrate, NO$_3$	mg L^{-1}	0–460	±2.2%
OTT ecoLog 1,000	Temperature, T	°C	−25–70	±0.05%
	Level	m	0–10	±0.001
OTT MFpro	Flow velocity	m s^{-1}	0–3.04	±2%
	Water depth	m	0–3.05	±2%

The spectro::lyser with an optical path length (OPL) of 5 mm was used. Missing information was indicated as not available (n.a.).

works were filtered out, marked by rapid concentration shifts toward atmospheric values until equilibrium was reestablished. The quality-checked GHG, stream and water quality data were aggregated into hourly resolution, which also smoothed minor variabilities due to measurement uncertainties.

Because chamber headspace temperature data were partly unavailable, continuous stream water measurements were used as a proxy, which showed an overall good fit ($R^2 = 0.99$) with an approximate offset of 2°C.

The measured GHG concentrations in [ppm] were used to infer dissolved GHG concentrations in the stream water based on Henry's law solubility constant (H^{cp}) in [mol m^{-3} Pa^{-1}] (Sander, 2015; Sander et al., 2022)

$$c_w = H^{cp} \times p \tag{1}$$

with aqueous gas concentration in water c_w in [mol m^{-3}] and the partial pressure p in [Pa] of the respective gas in the gas phase in equilibrium. The van't Hoff equation was applied to calculate temperature-dependent Henry's law constants ($H^{cp}(T)$) after Sander (2015)

$$H^{cp}(T) = H^{\ominus} \times \exp\left(\frac{-\Delta_{sol}H}{R}\left(\frac{1}{T} - \frac{1}{T^{\ominus}}\right)\right) \tag{2}$$

with $H^{\ominus}$ in [mol m^{-3} Pa^{-1}] as the Henry's law solubility constant at standard temperature $T^{\ominus}$ in [K], the expression $\Delta_{sol}H$ as the molar enthalpy of dissolution in [J mol^{-1}] of the respective gas, and R as the ideal gas constant in [J mol^{-1} K^{-1}].

Hourly air-water GHG fluxes F in [mol m^{-2} h^{-1}] were estimated after

$$F = (c_w - c_a) \times k \tag{3}$$

using the gas concentration difference in water (c_w) and ambient air (c_a) in [mol m^{-3}] and the gas exchange velocity (k) in

[m h^{-1}] (Wanninkhof et al., 2009; Raymond et al., 2012). Molar masses of CO$_2$, CH$_4$, and N$_2$O were used to transform fluxes to [g m^{-2} h^{-1}].

Estimations of k for each GHG were calculated according to

$$k = k_{600}\left(\frac{600}{Sc}\right)^{-0.5} \tag{4}$$

with standardized k values to the dimensionless and temperature-dependent Schmidt number (Sc) of 600 (k_{600}) divided by 24 for hourly resolution using an empirical equation after Raymond et al. (2012) with flow velocities (V) in [m s^{-1}] and the slope (S) in [m m^{-1}]:

$$k_{600} = V \times S^{0.76} \times 951.5 \tag{5}$$

For full GHG balance over the observation period, measurement gaps were interpolated linearly. Hourly averaged fluxes of CH$_4$ and N$_2$O were multiplied by the respective GWPs of 27.2 and 273 and added to the CO$_2$ fluxes to obtain a GHG balance in CO$_2$-equivalents. Moreover, to investigate the effects of lower sampling frequencies on the total GHG balance, the dataset was also randomly sampled once a day and three times (Monday, Wednesday, Friday) or once (Wednesday) per week during the daytime between 9 AM and 5 PM, with linear interpolation between the sampled data.

3 Results

3.1 Review of maintaining the measuring setup

The GHG monitoring setup was continuously operated over ~5 months, from March 31 to August 25, 2023. Via the installed network camera and remote laptop access, overall conditions (e.g.,
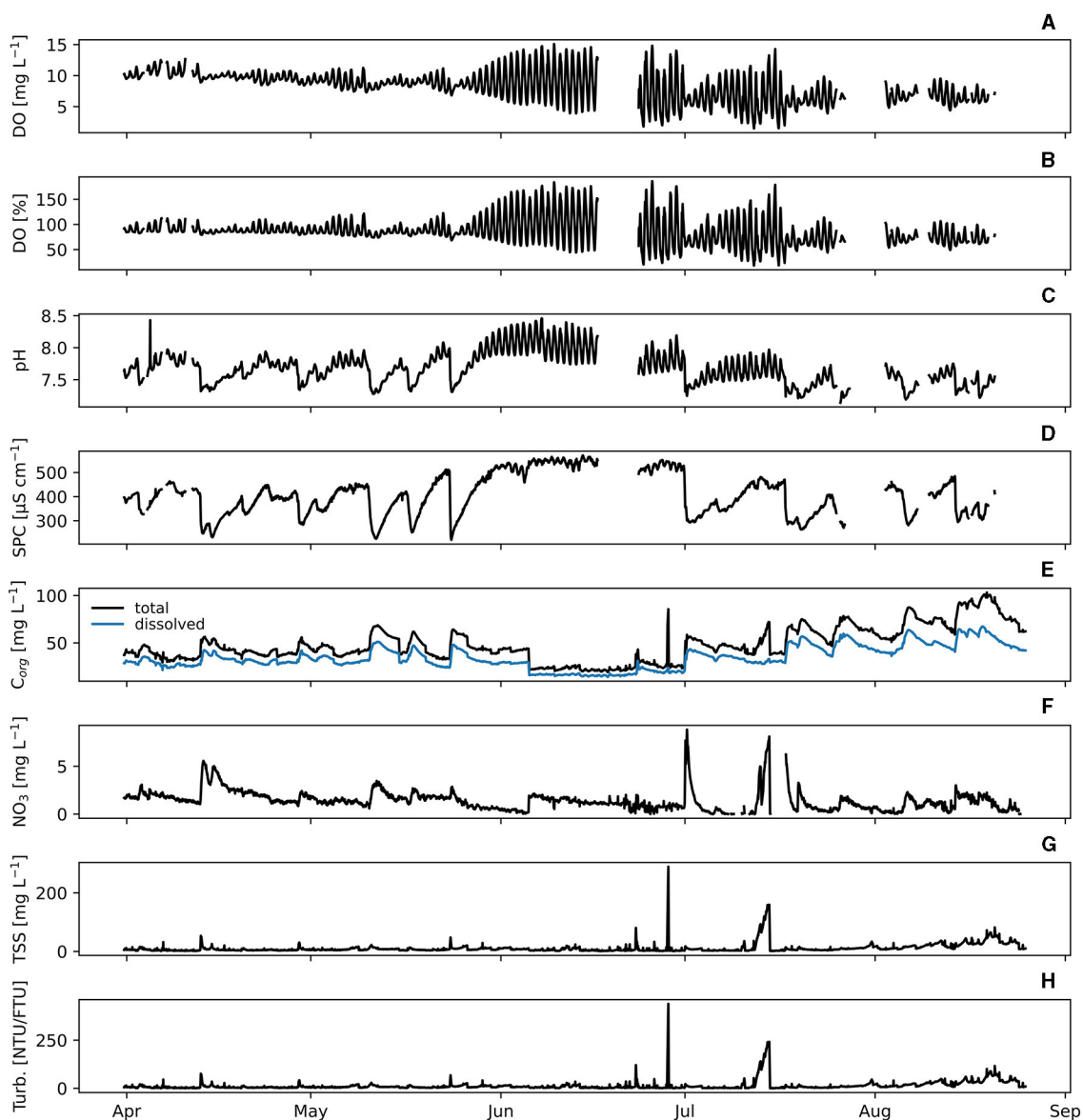
FIGURE 6
Overview of hourly averaged water chemistry parameters including **(A)** dissolved oxygen (DO) concentration [mg L^{-1}] and **(B)** saturation [%], **(C)** specific conductance (SPC) [μS cm^{-1}], **(D)** pH [-], **(E)** dissolved and total organic carbon (C_{org}) [mg L^{-1}], **(F)** nitrate (NO_3) [mg L^{-1}], and **(G)** total suspended solids (TSS) [mg L^{-1}], and **(H)** turbidity (turb.) [NTU/FTU] between March 31 and August 25, 2023. In the subfigures **(A–D)**, gaps indicate measurement failures or filtered outliers. In **(E–H)**, differences between hourly averaged and consecutive measurements were used to filter out significant outliers ($\pm$3 standard deviations), with values of 0 shown as data gaps.

stream water level, pumping rates) at the measurement site and of the measurements were controlled daily. The performance of the energy trailer, including energy supply and fuel status, was checked on a regular basis. Automated warning messages were sent in cases of low battery charge, fuel status, or other errors. Next to remote controls, on-site checkups and cleaning procedures were performed two to three times per week (mainly on Monday, Wednesday, and Friday).

Due to generally high DOC and POC concentrations in the HAS stream, fine organic matter accumulated on the in-stream probes and the plastic mesh grid of the pump, which were gently cleaned with a brush. The deposition of fine sediments

also in the garden hose and air-water equilibrator tubes caused a gradual decrease in pumping rates. Low pumping pressure directly influenced spraying behaviors through the spray nozzles into the air-water equilibration chamber with fewer fine droplets at lower flow rates. Therefore, once per week, the equilibration chamber was disconnected, and the garden hose was flushed by turning the water pump on and off several times. Additionally, the tubes and the equilibration chamber were cleaned with a brush. When pumping rates decreased to 2.0 L/min even after cleaning, the garden hose was replaced, and initial pumping rates could be re-established. Pumping rates could be kept relatively stable between 2.0 and 3.0 L min^{-1}. Only once the pumping rate

FIGURE 7
Overview of **(A)** measured water levels [m], including consecutive numbers of peaks (1−19), and water temperatures [°C] together with hourly cumulative precipitation [mm h^{-1}] data from the weather station Attenkam (data source: Deutscher Wetterdienst, 2023) in comparison with **(B)** hourly averaged greenhouse gas (GHG) concentration measurements in parts per million (ppm) (black lines) and flux estimations [mg m^{-2} h^{-1}] (gray line) of CO_2, **(C)** CH_4 and **(D)** N_2O **(D)** [ppm] in dry air from March 31 to August 25, 2023. In **(E)**, inferred gas exchange velocity (k) values [m h^{-1}] of CO_2 are presented, which are also representative of the other two GHGs.

dropped to 1.7 L min^{-1}, but could be increased to 2.6 L min^{-1} after cleaning.

Shorter GHG measurement disruptions mainly occurred due to regularly performed maintenance works or measurement stops in favor of other field experiments. Also temporally rising water levels in the water-air equilibration chamber, freezing sample air tubes at cool temperatures in April 2023, power supply failures of the energy trailer, or malfunction of the field laptop (for LI-840A data) caused occasional GHG measurement data losses. Only 11 and 22% of CH_4 and N_2O, and CO_2 concentration data were filtered out or not measured, respectively. The water switch and the 3/2-way solenoid valves were activated once water entered sample air tubes due to high equilibration chamber water levels before the vent was installed, which successfully prevented water suction into the GHG analyzers.

3.2 Environmental site parameters

An overview of measured site parameters and precipitation events is shown in Figures 6A–H, 7A. Generally, cooler stream water temperatures were observed in April with a minimum of 1.4°C, which increased to a maximum of 27.2°C in June and ranged between 11.4 and 23.7°C in July and August. The water temperatures showed strong diurnal patterns with higher temperatures during the day. Stream water levels were highly variable and increased due to several rainfall events during the observed period, which could be assigned to 19 distinct peaks (Figure 7A). The lowest cumulative precipitation (23.3 mm) and water level (0.44 m) were recorded in June. In the months May, July and August, higher water levels of up to 1.02 m were observed as a result of elevated cumulative precipitation with 105.4, 109.6, and 104 mm, respectively.

The Pro DSS multiprobe experienced several measurement failures, which resulted in data gaps for dissolved oxygen (DO), pH, and specific conductance (SPC). During the observed time period, DO concentrations and saturations varied between 1.5 and 15.1 (mean $\pm$std: 8.3 $\pm$2.4) mg L^{-1}, and 18.1 and 186.1 (86.2 $\pm$25.7) %, respectively. We observed pronounced day-night cycles, particularly in the months of June and July (Figures 6A, B). Measured pH values were constantly neutral to alkaline and ranged from 7.1 to 8.5 (7.7 $\pm$0.2). Significant drops in pH occurred after rainfall events at rising stream water levels and showed similar diurnal patterns related to DO and CO_2 (Figures 6C, 7A, B). Also, Similar to pH, SPC strongly dropped at hydrologic events, ranging between 220.7 and 571.2 (407.7 $\pm$84.7) μS cm^{-1} (Figure 6D), with overall highest values at baseflow conditions. Carbon concentrations varied between 14.1 and 67.3 (34.8 $\pm$12.4), and 19.2 and 103.2 (48.1 $\pm$18.5) mg L^{-1} for dissolved (DOC) and total organic carbon (TOC) (Figure 6E) and continuously increased from July to the end of August. As for DOC and TOC, concentrations of nitrate (NO_3^-) tended to increase with stream water levels and ranged between 0.1 and 8.8 (1.4 $\pm$1.0) mg L^{-1} (Figure 6F) but did not show pronounced diurnal variations. Total suspended solids (TSS) and turbidity varied between 0.9 and 289.2 (11.1 $\pm$16.2) mg L^{-1} and 0 and 438.5 (13.3 $\pm$24.0) in the Formazine Turbidity Unit (FTU) or Nephelometric Turbidity Unit (NTU) (Figures 6G, H).

3.3 Continuous GHG measurements in high temporal resolution

To show the potential of the continuous GHG measurement setup to resolve GHG (i.e., CO_2, CH_4, and N_2O) dynamics in high temporal resolution, the presented dataset covers different hydrologic stream conditions during a cooler spring and warmer summer period from March 31 to August 25, 2023, including low, moderate, and also heavier thunderstorm-related rainfall and resulting discharge events. Measured GHG concentrations and estimated fluxes (Table 3) based on Equations (1–5) were strongly influenced by the magnitude, frequency, and timing of precipitation events and associated HAS water level dynamics. Over the overserved period, CO_2 and CH_4 concentrations were constantly highly oversaturated, whereas N_2O showed generally lower levels of oversaturation and even atmospheric equilibrium and undersaturation in situations with low stream water levels (Figures 7A–D). Estimated k values for GHG flux estimations ranged between 0.004 and 0.099 (0.023 $\pm$0.017) m h^{-1} (Figure 7E).

At cooler weather conditions and prior to the prolonged dry period in June, concentrations of CO_2, CH_4, and N_2O peaked shortly after rising water levels associated with rainfall events with maximum values of 7,078.1, 580.6, and 2.0 ppm, respectively, followed by a significant drop when water levels were still increasing. Smaller rainfall events only showed minor impacts on in-stream GHG concentrations. Diurnal CO_2 patterns were particularly visible at lower water levels, with lower values occurring during the day and higher at night. Overall, GHG concentration and gas exchange velocity influenced the estimated

temporal dynamics of GHG fluxes, which highly depend on stream water level and associated stream velocity (Figures 5, 7B–E).

At low stream water levels, particularly in the dry period from May 24 and June 19, CO_2 and CH_4 concentrations and fluxes showed regular and pronounced day-night cycles (Figures 7A–C), but such patterns were less visible for N_2O concentrations and fluxes. Overall, the magnitude of diurnal variation of GHG concentration was higher than the variation of fluxes, following generally limited gas exchange in periods of low water levels indicated by low values of k (Figures 7A–E).

More frequent mainly thunder-storm related precipitation events occurred in the warm period from the end of June to the end of August, which positively affected the magnitude of GHG concentrations and emissions mainly following an increase in stream water levels. During the first precipitation event on June 22, with only a moderate increase in water level (peak 9), CO_2, CH_4, and N_2O concentrations strongly increased to 8,040.5, 1133.3, and 2.9 ppm. A following significant water level rise on July 1 (peak 10) caused the highest concentrations of CH_4 (1,478.6 ppm) and N_2O (9.9 ppm) during the entire observation period, whereas CO_2 only increased up to 6,948.9 ppm. In the period until mid-July, following decreasing water levels, diurnal patterns of GHG concentrations and emissions were most obvious. Toward the end of the observation period (25 August onwards), the stream water level impacts (peak 17–19) on corresponding GHG concentrations and emissions were less pronounced than in previous events.

3.4 GHG hysteresis loops at selected water level peaks

Water level peaks 6, 10, and 16 (see Figure 7A) with similar heights were selected to show the development of hysteresis loops of CO_2, CH_4, and N_2O concentrations and SPC compared to water level heights during a cool and wet (CW) period in May (Figures 8A, D, G, J), warm conditions in June after a dry period (WD) (Figures 8B, E, H, K), and warm and wet (WW) conditions in August (Figures 8C, F, I), respectively.

During the event (peak 6) in the CW, CO_2 and CH_4 concentrations were characterized by an initial rapid increase, followed by a decrease to water levels around 0.7 m and a second peak at rising water levels up to 0.8 m (Figures 8A, D). The second CO_2 peak was higher, whereas CH_4 concentrations showed similar values to the first peak and decreased with increasing water levels. Simultaneously, SPC showed relatively constant values up to a water level of 0.6 m, with a subsequent decrease until the water level peak was reached. CO_2 and CH_4, as well as SPC, fell sharply at the highest water levels, with concentrations approaching pre-event concentrations as water levels fell. While the temporal trends of CO_2, CH_4, and SPC followed a clockwise pattern, N_2O concentrations showed an anti-clockwise trend with a relatively narrow hysteresis, with increasing and decreasing concentrations following rising and falling water levels, respectively (Figures 8G, J).

During the rainfall event in warm June after a prolonged dry period (peak 10), CO_2 and CH_4 concentrations followed a disproportionate increase in water levels, with the highest peaks at 0.6 to 0.7 m (Figures 8B, E). Thereafter, values decreased

TABLE 3 Overview of measured greenhouse gas (GHG) concentrations (hourly averaged) and estimated fluxes of CO_2, CH_4, and N_2O, including the mean, standard deviation (SD), minimum, and maximum between March 31 and August 25, 2023.

Parameter [unit]	Gas	Mean	Standard deviation	Minimum	Maximum
Concentration [ppm]	CO_2	4,504.9	1,610.8	1,413.3	9,959.1
	CH_4	392.3	99.7	210.7	1,478.6
	N_2O	0.7	0.8	0.2	9.9
Flux [mg m^{-2} h^{-1}]	CO_2-C	61.00	57.54	3.08	313.89
	CH_4-C	0.20	0.17	0.03	1.17
	N_2O-N	0.01	0.04	0.00	0.40
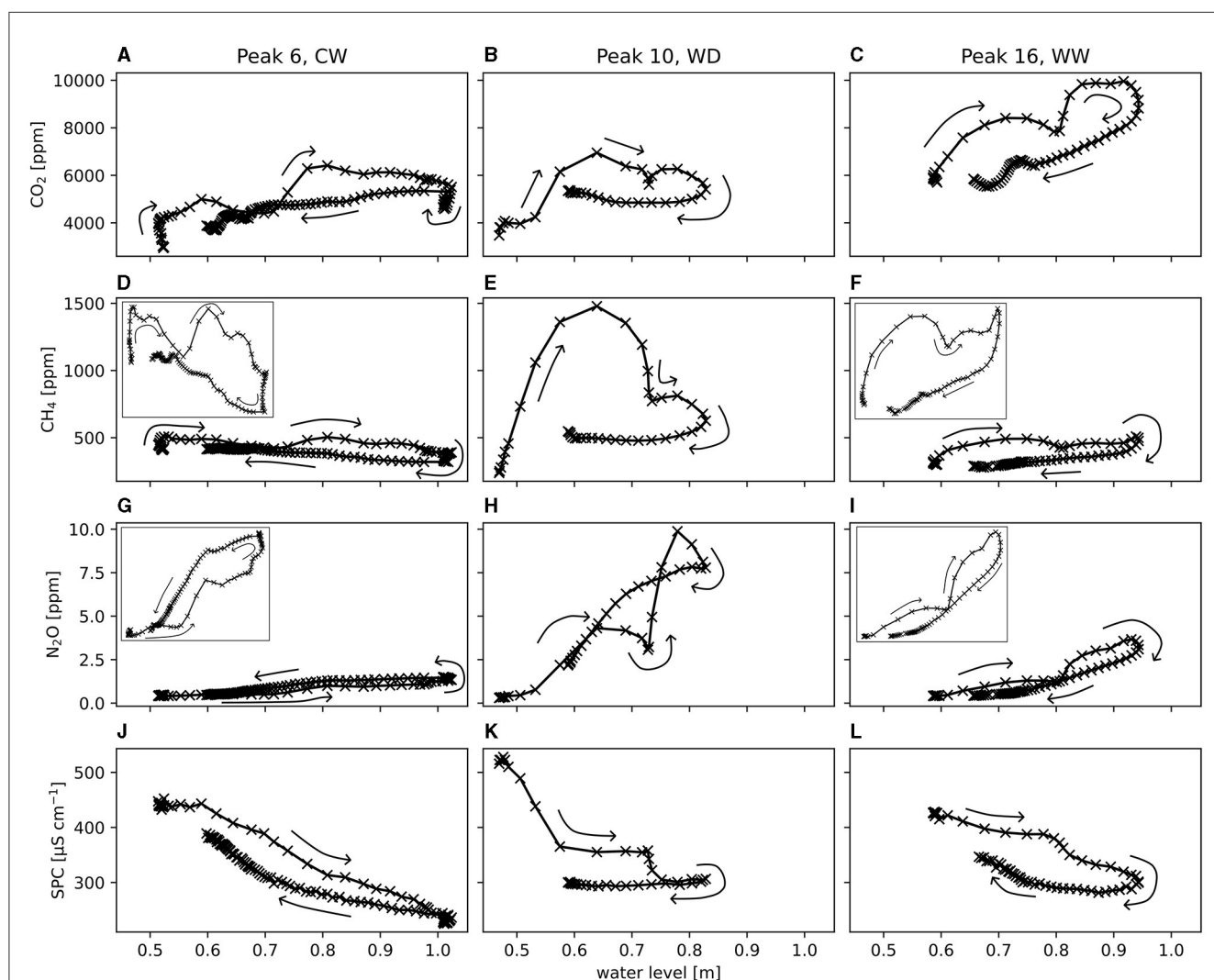
FIGURE 8
Hysteresis loops of the greenhouse gases (GHG) CO_2, CH_4, and N_2O in [ppm], and specific conductivity (SPC) in [μS cm^{-1}] of selected water level peaks (6, 10, and 16; see Figure 7), that occurred during cool and wet conditions (CW) (A, D, G, J), a warm period after drier conditions (WD) (B, E, H, K), and warm and wet conditions (WW) (C, F, I, L), respectively, in the observed time period between March 31 and August 25, 2023. In (D) and (F), and (G) and (I), zoomed-in plots are depicted to show the patterns of CH_4 and N_2O concentrations more clearly, respectively. Arrows indicate the temporal succession, and hourly averaged measurements are shown as an x.

significantly toward the water level maximum, including a second smaller peak between 0.7 and 0.8 m. CO_2 concentrations remained relatively constant on the falling limb at higher concentration levels. In contrast, N_2O peaks at rising water levels showed a similar timing but with a more significant second peak at high water levels (Figure 8H). In addition, the N_2O returned to levels close to pre-event concentrations. The SPC values were characterized by a strong decrease up to a water level of about 0.6 m, followed by more

constant values and a drop between 0.7 and 0.8 m. After reaching the maximum water level, the SPC values remained relatively constant at falling water levels, comparable to the trends observed for CO_2 and CH_4 (Figures 8B, E, K), while the N_2O concentration decreased strongly.

During the event in the WW period (peak 16), CO_2 and CH_4 concentration trends were similar to the CW conditions, with maximum concentrations occurring close to the highest water levels (Figures 8C, F). In contrast to CO_2 and CH_4, which had larger hysteresis effects, N_2O concentrations followed trends of increasing and decreasing water levels with relatively narrow hysteresis loops (Figure 8I). The trends of SPC values mostly followed the GHG concentrations, although they showed opposing trends to increasing and decreasing water levels (Figure 8L).

3.5 Greenhouse gas (GHG) balance

The cumulative GHG balance over the 140-day measurement period yielded a value of 762.2 (CO_2: 719.3, CH_4: 24.5, N_2O: 18.4) g m^{-2} CO_2-eq. GHG balances in context with rainfall events and significant water level rises showed an increased GHG balance of 449.5 (CO_2: 420.0, CH_4:13.5, N_2O: 16.0) g m^{-2} CO_2-eq compared to periods of reduced or no rainfall (total: 313.4, CO_2: 300.0, CH_4: 11.0, N_2O: 2.4 g m^{-2}) (Figure 9A). GHG budgets with lower sampling frequencies showed lower (daily) or higher (three days a week, weekly) values than the results from continuous monitoring, with the overall highest cumulative GHG budget for the weekly sampling (948.2 g m^{-2} CO_2-eq) (Figure 9B). Proportions of the respective GHGs were variable, whereas CO_2 showed the largest impact on the cumulative GHG balance.

4 Discussion

4.1 Technical aspects

The basic principle of our continuous GHG measurement setup, i.e., a water-air equilibrator connected to gas analyzers, was previously described and tested in the literature; however, these continuous measurement setups were optimized to perform with other water-equilibrator types, measure only selected GHGs or other gases, such as radon, or were operated in other aquatic ecosystems, e.g., groundwaters or marine environments (Gülzow et al., 2011; Santos et al., 2012; Gonzalez-Valencia et al., 2014; Webb et al., 2016; Durejka et al., 2019; Lacroix et al., 2021). To our knowledge, detailed descriptions of an automated measurement system for continuous and simultaneous CO_2, CH_4, and N_2O concentration measurements in headwater streams are presented for the first time. As shown in this study, we found the most important determinant factor for continuous measurements to be a permanent energy supply, which can be challenging without public power access. The described energy trailer provided sufficient energy for applying GHG measurements based on the spray chamber equilibration method, water chemistry measurements, and remote surveillance setup, which Durejka et al. (2019) saw as a major limitation.

The basic concept of a shower head water-air equilibration chamber, as used in this measurement setup, has been frequently applied in the past due to usually short equilibration response times, i.e., durations until equilibrium between sample water and chamber air is established, compared to other equilibration systems (Pierrot et al., 2009; Santos et al., 2012; Webb et al., 2016). In contrast with other air-water equilibrators, such as the marble and membrane type, the shower head equilibrator also shows lower risks of clogging, biofouling, or memory effects with possible influences on measured GHG concentrations (Santos et al., 2012; Webb et al., 2016). Based on our observations and other studies, sufficient inflow into the spray chamber is essential for fast equilibration times of dissolved gases (i.e., outgassing and dissolution of gases from and into sample water, respectively), which depends on the surface area of the sprayed water droplets as well as H^{cp}, k, and p of the respective gases, and the ratio of water and air volumes in the chamber (Schneider et al., 2007; Gülzow et al., 2011; Sander, 2015; Webb et al., 2016). Also, sufficient outflow is needed to avoid increased atmospheric equilibration of collected water at the bottom (Figure 4).

The primary efforts of this GHG measurement method were regular maintenance works dedicated to the constant accumulation of sediments and possible growth of microbial biofilms on inner tube walls and the equilibration chamber over pumping time and adverse effects on water inflow and outflow (Dinsmore et al., 2013; Campeau et al., 2017; Prijac et al., 2023; Pschenyckyj et al., 2023). However, the accumulation of fine particulate sediments and microbial growth in C-rich streams can also be expected to occur in other equilibration types, such as capillary membranes characterized by even longer equilibration times (Webb et al., 2016; Durejka et al., 2019). Response times of the presented system for continuous GHG monitoring with a shower head type equilibrator can be assumed to be comparable to other studies at similar pumping rates with CO_2 equilibration up to several minutes and for CH_4 up to several hours, as shown in Webb et al. (2016). In addition, water-air equilibrators lead to a water vapor-saturated sample air, which should be pre-dried to avoid possible condensation within the closed air loop and effects on the measurement performance due to spectral interferences between H_2O and measured GHGs (Gülzow et al., 2011; Santos et al., 2012; Webb et al., 2016). However, irregularly taken discrete samples collected by the headspace equilibration method after Raymond et al. (1997) showed comparable concentrations.

4.2 Scientific aspects

The presented high temporal variability of physicochemical water parameters, GHG concentrations, and estimated fluxes during a cooler spring and a warmer summer (April–August 2023), including a low precipitation period in June, indicate the importance of continuous and high-resolution GHG measurements in peatland headwater streams due to their strong dependence on rainfall events and connection to the surrounding catchment area (Dinsmore et al., 2013; Hotchkiss et al., 2015; Piatka et al., 2021).
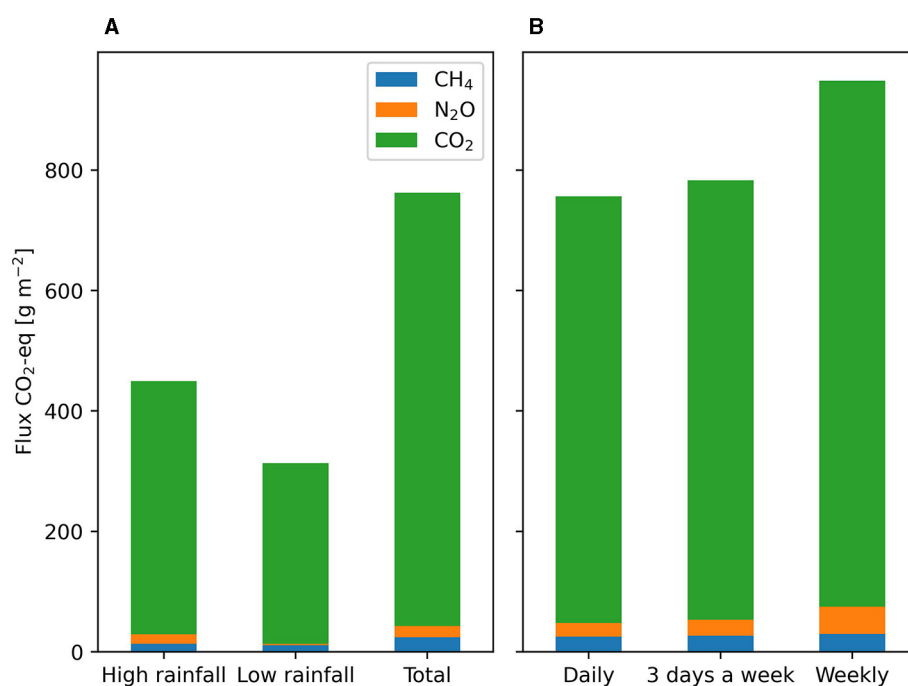
FIGURE 9
Stacked bar plots for the greenhouse gases (GHGs) CO_2 (green), CH_4 (blue), and N_2O (orange), which represented the CO_2-equivalent (CO_2-eq) fluxes in [g m^{-2}], with **(A)** contributions to the GHG budget during the low and high rainfall, and entire observation period, and **(B)** effects of different sampling frequencies [continuously and randomly daily, three-weekly (Monday, Wednesday, Friday), or weekly (Wednesday)] during the daytime between 9 AM and 5 PM.

During periods of low or no precipitation associated with low water levels, in-stream biogeochemical processes, and environmental parameters, such as higher photosynthetically active radiation (PAR) and water temperatures, were important drivers of diurnal trends in CO_2 concentrations and fluxes, and opposing trends in DO and pH (Figures 6A–C, 7A, B) (Song et al., 2018; Rocher-Ros et al., 2020; Attermeyer et al., 2021). During the day, when photosynthesis (P) (CO_2 sink and DO source) and respiration (R) (CO_2 source and DO sink) were active, CO_2 concentrations were lowest (but still above ambient concentrations), whereas the highest values were observed at night when only R is present (Hotchkiss et al., 2015; Piatka et al., 2021, 2022b). With successive rainfall events, these diurnal CO_2 cycles were strongly dampened, likely by increased k values at higher water levels and flow velocities and possibly by reduced PAR, hence P under cloudy conditions (Figures 7A, B, E) (Raymond et al., 2012; Piatka et al., 2022b). Higher stream pH during the day may also have shifted the dissolved inorganic carbon (DIC) equilibrium from CO_2 to bicarbonate (HCO_3^-) and carbonate (CO_3^{2-}) (Stumm and Morgan, 2012; Piatka et al., 2021, 2022a). However, as indicated by the consistently high CO_2 oversaturations, the in-stream CO_2 level was primarily fueled by allochthonous (i.e., external) sources from the surrounding catchment, with the direct input of CO_2-rich waters from the surrounding soils or the HZ, via the oxidation of CH_4 (Taillardat et al., 2022). Corresponding fluxes at low water levels were mainly controlled by changes in diurnal concentrations or increased k-values at slightly higher water levels [see Equation (3), Figures 7B, E].

Under low rainfall conditions, similar diurnal patterns with higher concentrations at night were also visible for CH_4, especially during the warm and dry summer in June, with diurnal variations up to more than 200 ppm and oversaturations constantly above 15,000%. Such large day-night cycles could be explained by accelerated microbial methanotrophic oxidation of CH_4 to CO_2 at higher photosynthetic O_2 concentrations and water temperatures during the day, which could contribute to the observed decreases in CH_4 concentrations (Taillardat et al., 2022). In addition, lower dissolved O_2 concentrations and prolonged anoxic conditions in the sediments at night could favor microbial CH_4 production (Bange et al., 2019; Piatka et al., 2021; Michaelis et al., 2022). As shown by Taillardat et al. (2022) using a combination of CH_4 concentration and C stable isotope analyses, and in other studies, high proportions of CH_4 in peatland streams can originate from anaerobic peatland soil pore water and methanogenic production, even at lower water levels (Hope et al., 2001; Bange et al., 2019). In contrast, the observed N_2O concentrations showed minor variations close to and even below the atmospheric equilibrium under low-flow conditions. In such oxygen-depleted peatland soils, N_2O is usually completely denitrified to N_2, with NO_3^- as an important N source (Butterbach-Bahl et al., 2013). Overall, the dynamics of the inferred CH_4 and N_2O fluxes were mainly driven by minor differences in k and concentration gradients between the atmosphere and stream water (Figures 7C–E).

Heavier and more frequent precipitation events resulted in significant water level increases, with distinct effects on the respective GHG concentrations and SPC values depending on the

environmental conditions, which varied between seasons, as shown by the hysteresis loops at selected water level peaks (Figures 8A–L). The hysteresis curves generally indicated complex relationships between GHG concentrations and water levels as a proxy for flow velocity and in-stream GHG concentrations resulting from hydrological characteristics and C and N turnover processes in the catchment area (Dinsmore and Billett, 2008; Feinson et al., 2016; Mehdi et al., 2021). All GHG concentrations were characterized by a rapid increase shortly after rainfall events. These findings could be due to CO_2, N_2O, and CH_4 leaching from peatland pore water and surrounding landscape surfaces during and after rainfall events with rising peatland water tables, as decreasing SPC values indicate water input from rainfall triggered subsurface flow and surface runoff (Dinsmore et al., 2010, 2013; Raymond et al., 2016; Cano-Paoli et al., 2019; Taillardat et al., 2022). An allochthonous GHG-rich source from the catchment can also be inferred from the clockwise and anticlockwise accretion-type hysteresis loops, while the two peaks on the rising hydrograph could indicate either two different GHG sources from the peatland-rich catchment, watershed-specific hydrological flow patterns or altered in-stream C and N cycling (Dinsmore and Billett, 2008; Raymond et al., 2016; Mehdi et al., 2021). However, a more pronounced effect of precipitation on CH_4 and N_2O concentrations was observed during the warm summer, especially after the prolonged dry period (Figures 7A, C, D). Higher temperatures may have resulted in an accelerated microbial CH_4 production and subsequent accumulation under mainly anoxic conditions in water-logged and organic carbon-rich peatland pore waters, while more N_2O may have been produced during linked nitrification and denitrification processes from dissolved inorganic nitrogen species in the stream or peatland sediments (Drösler et al., 2008; Bouillon et al., 2012; Bridgham et al., 2013; Quick et al., 2019; Zhang et al., 2022). Relative to concentrations at lower water levels, in-stream CO_2 was less affected by rainfall events than N_2O and CH_4 due to anaerobic conditions in the peatland pore water, limiting microbial respiration (Drösler et al., 2008). However, the observed increase in CO_2 concentrations could be due to the input and oxidation of methane-rich peatland porewater, increasing DOC and TOC contents in the stream leached from the surrounding landscape as a C source for microbial turnover, and lower photosynthetic activities at lower PAR as compared to clear sky conditions (Figures 6E, 7B) (Dinsmore et al., 2013; Raymond et al., 2016; Piatka et al., 2021, 2022b; Taillardat et al., 2022). After reaching their maximum, significant decreases in GHG concentrations are probably related to reduced input of peatland soil water into the stream after the precipitation event or could be partially explained by dilution effects with rainwater and depletion of GHGs in the sediment pore waters (Hope et al., 2001; Billett et al., 2004; Wallin et al., 2010; Taillardat et al., 2022). The latter could also explain lower CH_4 and N_2O peaks following precipitation events in close temporal proximity, as observed mainly in the warmer summer (Figures 7A–D).

Discrete water velocity measurements in this study were mainly performed during the cooler spring. Growing macrophytes and lower water levels in the warmer period could positively affect in-stream turbulence and k rates (Tseng and Tinoco, 2020). Therefore, estimated GHG fluxes and budgets based on the applied empirical

k-determinations may contain prediction uncertainties and lead to a substantial underestimation of inferred GHG fluxes and budgets due to the low stream slope. However, increased gas exchange fluxes could be derived for all GHGs at higher water flow velocities, largely masking changes in GHG concentrations (Figures 7B–D) (Raymond et al., 2012; Hall Jr and Ulseth, 2020).

The calculated budgets for all GHGs show that CO_2 caused the largest contribution (94.4%), as also suggested in other studies with lower sampling frequencies; however, with possible significant underestimations of CH_4 losses via ebullition (Dinsmore et al., 2010, 2013; Hendriks et al., 2023). Particularly GHG emissions after rainfall events should be considered, as they contributed 59% to the total budget, while covering only 31% of the observation period. Moreover, the contribution of N_2O to the GHG budget became similar to the share of CH_4 due to the high GWP of 273, which highlights considering all three GHGs in budget calculations. Notably, lower sampling intervals might lead to severe over- or underestimations of GHG emissions and budgets, as already suggested in terrestrial studies, which might especially become relevant on landscape scales (Figure 9B) (Smith and Dobbie, 2001; Parkin, 2008; Barton et al., 2015)

5 Conclusion

In this work, we present the technical setup for long-term continuous measurements of CO_2, N_2O, and CH_4 concentrations in headwater stream ecosystems, including detailed descriptions of the measurement devices and overall sampling design, performance, and maintenance experiences, as well as the applied mathematical formulae for GHG flux calculations. Based on the presented dataset, we could also highlight the high potential of simultaneous and high-resolution measurements of CO_2, CH_4, and N_2O concentration and respective flux and GHG budget assessments in peatland-dominated stream ecosystems due to their short-term variability, especially after heavy precipitation events. In a next step, GHG calibration procedures and response time characterization of the measurement system should be applied to assess further the quality and uncertainty of the GHG flux quantification from aquatic systems. Also, direct k determination based on adding inert gases (e.g., argon) and conservative tracers (e.g., NaCl) could improve inferred GHG flux estimations at different hydrological conditions (Hall Jr and Madinger, 2018). With our peatland stream water study, we could demonstrate the importance of continuous and high temporal resolution GHG datasets to improve our understanding of the processes, also in relation to *in-situ* vs. *ex-situ* GHG production in combination with water quality parameters. As aquatic ecosystems act as hotspots of C and N cycling, it will be crucial to understand short-term (daily, seasonal) and long-term (years and longer) GHG dynamics under changing land management and climatic conditions. Following the setup presented in this work, more continuous and simultaneous concentration measurements of all three GHG and flux estimations could be carried out in various aquatic ecosystems, including ponds, ditches, and marine ecosystems. Combining these measurements can contribute to a better understanding of GHG sources and pathways. Complementary measurements of key

meteorological (e.g., solar radiation, wind speed, air temperature, atmospheric pressure) and aquatic environmental parameters (e.g., water temperature, pH, DOC, POC) can further improve our understanding of C and N cycles and their impact on GHG losses to the atmosphere. Incorporating continuous stable isotope measurements of C and N could help to decipher turnover processes and identify sources and sinks. More research is needed in headwater streams and larger rivers to better constrain exchange processes between terrestrial and aquatic ecosystems controlling gaseous, dissolved, and particulate C and N transport and gaseous fluxes at the landscape scale.

Data availability statement

The original contributions presented in the study are included in the article, further inquiries can be directed to the corresponding author.

Author contributions

DP: Data curation, Formal analysis, Investigation, Methodology, Project administration, Validation, Visualization, Writing – original draft, Writing – review & editing. RN: Investigation, Methodology, Project administration, Writing – review & editing. RM: Writing – review & editing. FE: Methodology, Writing – review & editing. GW: Methodology, Writing – review & editing. FN: Methodology, Writing – review & editing. RK: Conceptualization, Funding acquisition, Methodology, Project administration, Supervision, Writing – review & editing.

Funding

Acknowledgments

Conflict of interest

The authors declare that the research was conducted in the absence of any commercial or financial relationships that could be construed as a potential conflict of interest.

Publisher's note

All claims expressed in this article are solely those of the authors and do not necessarily represent those of their affiliated organizations, or those of the publisher, the editors and the reviewers. Any product that may be evaluated in this article, or claim that may be made by its manufacturer, is not guaranteed or endorsed by the publisher.

References

Aho, K. S., and Raymond, P. A. (2019). Differential response of greenhouse gas evasion to storms in forested and wetland streams. *J. Geophys. Res.* 124, 649–662. doi: 10.1029/2018JG004750

Alexandrov, G. A., Brovkin, V. A., Kleinen, T., and Yu, Z. (2020). The capacity of northern peatlands for long-term carbon sequestration. *Biogeosciences* 17, 47–54. doi: 10.5194/bg-17-47-2020

Allan, J. D. (2004). Landscapes and riverscapes: The influence of land use on stream ecosystems. *Annu. Rev. Ecol. Evol. Syst.* 35, 257–284. doi: 10.1146/annurev.ecolsys.35.120202.110122

Appling, A. P., Read, J. S., Winslow, L. A., Arroita, M., Bernhardt, E. S., Griffiths, N. A., et al. (2018). The metabolic regimes of 356 rivers in the United States. *Scientific Data* 5, 180292. doi: 10.1038/sdata.2018.292

Attermeyer, K., Casas-Ruiz, J. P., Fuss, T., Pastor, A., Cauvy-Frauni,é, S., Sheath, D., et al. (2021). Carbon dioxide fluxes increase from day to night across European streams. *Communications Earth Environm.* 2, 118. doi: 10.1038/s43247-021-00192-w

Bade, D. L. (2009). "Gas exchange at the air–water interface," in *Encyclopedia of Inland Waters*, eds. G. E. Likens. Oxford: Academic Press, 70–78. doi: 10.1016/B978-012370626-3.00213-1

Bange, H. W., Sim, C. H., Bastian, D., Kallert, J., Kock, A., Mujahid, A., et al. (2019). Nitrous oxide (N2O) and methane (CH4) in rivers and estuaries of northwestern Borneo. *Biogeosciences* 16, 4321–4335. doi: 10.5194/bg-16-4321-2019

Barton, L., Wolf, B., Rowlings, D., Scheer, C., Kiese, R., Grace, P., et al. (2015). Sampling frequency affects estimates of annual nitrous oxide fluxes. *Sci. Rep.* 5, 15912. doi: 10.1038/srep15912

Battin, T., Luyssaert, S., Kaplan, L., Audfenkampe, A., Richter, A., and Tranvik, L. (2009). The boundless carbon cycle. *Nat. Geosci.* 2, 598–600. doi: 10.1038/ngeo618

Battin, T. J., Lauerwald, R., Bernhardt, E. S., Bertuzzo, E., Gener, L. G., Hall, R. O., et al. (2023). River ecosystem metabolism and carbon biogeochemistry in a changing world. *Nature* 613, 449–459. doi: 10.1038/s41586-022-05500-8

Bayerisches Landesamt für Umwelt (2023). Available online at: www.lfu.bayern.de (accessed 31 August, 2023).

Berg, P., and Pace, M. (2017). Continuous measurement of air–water gas exchange by underwater eddy covariance. *Biogeosciences* 14, 5595–5606. doi: 10.5194/bg-14-5595-2017

Bernrieder, M. (2003). Renaturierung von land und forstwirtschaftlich genutzten Hoch und Übergangsmoorflächen. *Laufener Seminarbeiträge* 1:121.

Billett, M. F., and Harvey, F. H. (2013). Measurements of CO2 and CH4 evasion from UK peatland headwater streams. *Biogeochemistry* 114, 165–181. doi: 10.1007/s10533-012-9798-9

Billett, M. F., and Moore, T. R. (2008). Supersaturation and evasion of CO2 and CH4 in surface waters at Mer Bleue peatland, Canada. *Hydrol. Process.* 22, 2044–2054. doi: 10.1002/hyp.6805

Billett, M. F., Palmer, S. M., Hope, D., Deacon, C., Storeton-West, R., Hargreaves, K. J., et al. (2004). Linking land-atmosphere-stream carbon fluxes in a lowland peatland system. *Global Biogeochem. Cycles* 18, GB1024. doi: 10.1029/2003GB002058

Blodau, C. (2011). "Thermodynamic control on terminal electron transfer and methanogenesis, aquatic redox chemistry," in *ACS Symposium Series*. Washington, D.C.: American Chemical Society, 65–83.

Bouillon, S., Yambél,é, A., Spencer, R. G. M., Gillikin, D. P., Hernes, P. J., Six, J., et al. (2012). Organic matter sources, fluxes and greenhouse gas exchange in the Oubangui River (Congo River basin). *Biogeosciences* 9, 2045–2062. doi: 10.5194/bg-9-2045-2012

Bridgham, S. D., Cadillo-Quiroz, H., Keller, J. K., and Zhuang, Q. (2013). Methane emissions from wetlands: biogeochemical, microbial, and modeling perspectives from local to global scales. *Glob. Chang. Biol.* 19, 1325–1346. doi: 10.1111/gcb.12131

Butterbach-Bahl, K., Baggs, E. M., Dannenmann, M., Kiese, R., and Zechmeister-Boltenstern, S. (2013). Nitrous oxide emissions from soils: how well do we understand the processes and their controls? *Philos. Trans. R. Soc. Lond. B Biol. Sci.* 368, 20130122. doi: 10.1098/rstb.2013.0122

Campeau, A., Bishop, K., Billett, M., Garnett, M., Laudon, H., Leach, J., et al. (2017). Aquatic export of young dissolved and gaseous carbon from a pristine boreal fen: implications for peat carbon stock stability. *Glob. Chang. Biol.* 23, 13815. doi: 10.1111/gcb.13815

Cano-Paoli, K., Chiogna, G., and Bellin, A. (2019). Convenient use of electrical conductivity measurements to investigate hydrological processes in Alpine headwaters. *Sci. Total Environm.* 685, 37–49. doi: 10.1016/j.scitotenv.2019.05.166

Deutscher Wetterdienst (2023). Available online at: https://opendata.dwd.de/climate_environment/CDC/observations_germany/climate/multi_annual/mean_91-20/ (accessed September 9, 2023).

Dinsmore, K., Billett, M., Skiba, U., Rees, R., Drewer, J., and Helfter, C. (2010). Role of the aquatic pathway in the carbon and greenhouse gas budgets of a peatland catchment. *Glob. Chang. Biol.* 16, 2750–2762. doi: 10.1111/j.1365-2486.2009.02119.x

Dinsmore, K. J. (2008). *Atmosphere-Soil-Stream Greenhouse Gas Fluxes From Peatlands. (PhD Thesis)*. Edinburgh: University of Edinburgh.

Dinsmore, K. J., and Billett, M. F. (2008). Continuous measurement and modeling of CO2 losses from a peatland stream during stormflow events. *Water Resour. Res.* 44, 7284. doi: 10.1029/2008WR007284

Dinsmore, K. J., Billett, M. F., and Dyson, K. E. (2013). Temperature and precipitation drive temporal variability in aquatic carbon and GHG concentrations and fluxes in a peatland catchment. *Glob. Chang. Biol.* 19, 2133–2148. doi: 10.1111/gcb.12209

Downing, J. A., Cole, J. J., Duarte, C. M., Middelburg, J. J., Melack, J. M., Prairie, Y. T., et al. (2012). Global abundance and size distribution of streams and rivers. *Inland Waters* 2, 229–236. doi: 10.5268/IW-2.4.502

Drösler, M., Freibauer, A., Christensen, T. R., and Friborg, T. (2008). "Observations and status of peatland greenhouse gas emissions in Europe," in *The Continental-Scale Greenhouse Gas Balance of Europe*, eds. A. J. Dolman, R. Valentini and A. Freibauer. New York: Springer New York, New York, 243–261. doi: 10.1007/978-0-387-76570-9_12

Durejka, S., Gilfedder, B. S., and Frei, S. (2019). A method for long-term high resolution (222)Radon measurements using a new hydrophobic capillary membrane system. *J. Environ. Radioact.* 208–209, 105980. doi: 10.1016/j.jenvrad.2019.05.012

Evans, C., Renou-Wilson, F., and Strack, M. (2015). The role of waterborne carbon in the greenhouse gas balance of drained and re-wetted peatlands. *Aquat. Sci.* 78, 447. doi: 10.1007/s00027-015-0447-y

Feinson, L. S., Gibs, J., Imbrigiotta, T. E., and Garrett, J. D. (2016). Effects of land use and sample location on nitrate-stream flow hysteresis descriptors during storm events. *JAWRA* 52, 1493–1508. doi: 10.1111/1752-1688.12477

Frolking, S., Talbot, J., Jones, M., Treat, C., Kauffman, J., Tuittila, E.-S., et al. (2011). Peatlands in the Earth's 21st century climate system. *Environm. Rev.* 19, 371–396. doi: 10.1139/a11-014

Gao, C., Sander, M., Agethen, S., and Knorr, K.-H. (2019). Electron accepting capacity of dissolved and particulate organic matter control CO2 and CH4 formation in peat soils. *Geochim. Cosmochim. Acta* 245, 266–277. doi: 10.1016/j.gca.2018.11.004

Gonzalez-Valencia, R., Magana-Rodriguez, F., Gerardo-Nieto, O., Sepulveda-Jauregui, A., Martinez-Cruz, K., Walter Anthony, K., et al. (2014). In situ measurement of dissolved methane and carbon dioxide in freshwater ecosystems by Off-axis integrated cavity output spectroscopy. *Environ. Sci. Technol.* 48, 11421–11428. doi: 10.1021/es500987j

Gülzow, W., Rehder, G., Schneider, B., Deimling, J. S., and Sadkowiak, B. (2011). A new method for continuous measurement of methane and carbon dioxide in surface waters using off-axis integrated cavity output spectroscopy (ICOS): an example from the Baltic Sea. *Limnol. Oceanography: Meth.* 9, 176–184. doi: 10.4319/lom.2011.9.176

Hall Jr, R. O., and Madinger, H. L. (2018). Use of argon to measure gas exchange in turbulent mountain streams. *Biogeosciences* 15, 3085–3092. doi: 10.5194/bg-15-3085-2018

Hall Jr, R. O., and Ulseth, A. J. (2020). Gas exchange in streams and rivers. *WIREs Water* 7, e1391. doi: 10.1002/wat2.1391

Hanson, R. S., and Hanson, T. E. (1996). Methanotrophic bacteria. *Microbiol. Rev.* 60, 439–471. doi: 10.1128/mr.60.2.439-471.1996

Harenda, K. M., Lamentowicz, M., Samson, M., and Chojnicki, B. H. (2018). "The role of peatlands and their carbon storage function in the context of climate change," in *Interdisciplinary Approaches for Sustainable Development Goals: Economic Growth, Social Inclusion and Environmental Protection*, eds. T. Zielinski, I. Sagan and W. Surosz. Cham: Springer International Publishing, 169–187.

Hendriks, L., Weideveld, S., Fritz, C., Stepina, T., Aben, R. C. H., Fung, N. E., et al. (2023). Drainage ditches are year-round greenhouse gas hotlines in temperate peat landscapes. *Freshwater Biol.* doi: 10.1111/fwb.14200

Hope, D., Palmer, S. M., Billett, M. F., and Dawson, J. J. C. (2001). Carbon dioxide and methane evasion from a temperate peatland stream. *Limnol. Oceanogr.* 46, 847–857. doi: 10.4319/lo.2001.46.4.0847

Höper, H., Augustin, J., Cagampan, J. P., Drösler, M., Lundin, L., Moors, E., et al. (2008). "Restoration of peatlands and greenhouse gas balances," in *Peatlands and Climate Change*, eds. M. Strack. Quebec: International Peat Society, 182–210.

Hornibrook, E. R. C., Bowes, H. L., Culbert, A., and Gallego-Sala, A. V. (2009). Methanotrophy potential versus methane supply by pore water diffusion in peatlands. *Biogeosciences* 6, 1491–1504. doi: 10.5194/bg-6-1491-2009

Hotchkiss, E. R., Hall Jr, R. O., Sponseller, R. A., Butman, D., Klaminder, J., Laudon, H., et al. (2015). Sources and processes controlling CO2 emissions change with the size of streams and rivers. *Nat. Geosci.* 8, 696–699. doi: 10.1038/ngeo2507

Intergovernmental Panel on Climate Change (2021). *Climate Change 2021 The Physical Science Basis: Working Group I Contribution to the Sixth Assessment Report of the Intergovernmental Panel on Climate Change*. Cambridge: Cambridge University Press.

Intergovernmental Panel on Climate, C. (2022). *Global Warming of 1.5°C: IPCC Special Report on Impacts of Global Warming of 1.5°C above Pre-industrial Levels in Context of Strengthening Response to Climate Change, Sustainable Development, and Efforts to Eradicate Poverty*. Cambridge: Cambridge University Press.

Jennings, E., de Eyto, E., Moore, T., Dillane, M., Ryder, E., Allott, N., et al. (2020). From highs to lows: changes in dissolved organic carbon in a peatland catchment and lake following extreme flow events. *Water* 12, 2843. doi: 10.3390/w12102843

Jerz, H. (1979). Das Wolfratshausener Becken: seine glaziale Anlage und Übertiefung. *E&G Quaternary Sci. J.* 29, 63–70. doi: 10.3285/eg.29.1.06

Joosten, H., Tanneberger, F., and Moen, A. (2017). "Mires and peatlands of Europe," in *Status, Distribution and Conservation*. Stuttgart: Schweizerbart.

Julian, J. C. D., Billett, M. F., Hope, D., Palmer, S. M., and Claire, M. D. (2004). Sources and sinks of aquatic carbon in a peatland stream continuum. *Biogeochemistry* 70, 71–92. doi: 10.1023/B:BIOG.0000049337.66150.f1

Kasimir-Klemedtsson, Å., Klemedtsson, L., Berglund, K., Martikainen, P., Silvola, J., and Oenema, O. (1997). Greenhouse gas emissions from farmed organic soils: a review. *Soil Use Manage.* 13, 245–250. doi: 10.1111/j.1475-2743.1997.tb00595.x

Kaule, G., and Peringer, A. (2015). *Die Entwicklung der Übergangs-und Hochmoore im südbayerischen Voralpengebiet im Zeitraum 1969 bis 2013 unter Berücksichtigung von Nutzungs-und Klimagradienten*. Augsburg: Bayerisches Landesamt für Umwelt.

Lacroix, E., Donato, P., Lafortune, S., Caumon, M.-C., Barres, O., Liu, X., et al. (2021). In situ continuous monitoring of dissolved gases (N2, O2, CO2, H2) prior to H2 injection in an aquifer (Catenoy, France) by on-site Raman and infrared spectroscopies: instrumental assessment and geochemical baseline establishment. *Analytical Meth.* 13, 9. doi: 10.1039/D1AY01063H

Liu, H., Wrage-Mönnig, N., and Lennartz, B. (2020). Rewetting strategies to reduce nitrous oxide emissions from European peatlands. *Commun. Earth Environm.* 1, 17. doi: 10.1038/s43247-020-00017-2

Lyu, Z., Shao, N., Akinyemi, T., and Whitman, W. B. (2018). Methanogenesis. *Curr. Biol.* 28, R727–R732. doi: 10.1016/j.cub.2018.05.021

Maljanen, M., Sigurdsson, B. D., Guð*mundsson, J., Óskarsson, H., Huttunen, J. T., and Martikainen, P.J. (2010). Greenhouse gas balances of managed peatlands in the Nordic countries – present knowledge and gaps. *Biogeosciences* 7, 2711–2738. doi: 10.5194/bg-7-2711-2010

Marzadri, A., Amatulli, G., Tonina, D., Bellin, A., Shen, L. Q., Allen, G. H., et al. (2021). Global riverine nitrous oxide emissions: The role of small streams and large rivers. *Sci. Total Environm.* 776, 145148. doi: 10.1016/j.scitotenv.2021.145148

Mehdi, B., Schürz, C., Grath, B., and Schulz, K. (2021). Storm event impacts on in-stream nitrate concentration and discharge dynamics: A comparison of high resolution *in-situ* measured data with model simulations. *Sci. Total Environm.* 755, 143406. doi: 10.1016/j.scitotenv.2020.143406

Michaelis, T., Wunderlich, A., Coskun, Ö. K., Orsi, W., Baumann, T., and Einsiedl, F. (2022). High-resolution vertical biogeochemical profiles in the hyporheic zone reveal insights into microbial methane cycling. *Biogeosciences* 19, 4551–4569. doi: 10.5194/bg-19-4551-2022

Mwanake, R., Gettel, G., Ishimwe, C., Wangari, E., Butterbach-Bahl, K., and Kiese, R. (2022). Basin-scale estimates of greenhouse gas emissions from the Mara River, Kenya: Importance of discharge, stream size, and land use/land cover. *Limnol. Oceanogr.* 67, 1776–1793. doi: 10.1002/lno.12166

Mwanake, R., Gettel, G., Wangari, E., Butterbach-Bahl, K., and Kiese, R. (2023). Interactive effects of catchment mean water residence time and agricultural area on water physico-chemical variables and GHG saturations in headwater streams. *Front. Water* 5, 1220544. doi: 10.3389/frwa.2023.1220544

Parkin, T. B. (2008). Effect of sampling frequency on estimates of cumulative nitrous oxide emissions. *J. Environ. Qual.* 37, 1390–1395. doi: 10.2134/jeq2007.0333

Piatka, D. R. (2022). *Dissolved Oxygen and Carbon Phase Turnover in Terrestrial Freshwater Ecosystems with their Stable Isotopes as Process Indicators* (PhD thesis). Erlangen: Friedrich-Alexander-Universität Erlangen-Nürnberg.

Piatka, D. R., Frank, A. H., Köhler, I., Castiglione, K., van Geldern, R., and Barth, J. A. C. (2022a). Balance of carbon species combined with stable isotope ratios show critical switch towards bicarbonate uptake during cyanobacteria blooms. *Sci. Total Environm.* 807, 151067. doi: 10.1016/j.scitotenv.2021.151067

Piatka, D. R., Venkiteswaran, J. J., Uniyal, B., Kaule, R., Gilfedder, B., and Barth, J. A. C. (2022b). Dissolved oxygen isotope modelling refines metabolic state estimates of stream ecosystems with different land use background. *Sci. Rep.* 12, 10204. doi: 10.1038/s41598-022-13219-9

Piatka, D. R., Wild, R., Hartmann, J., Kaule, R., Kaule, L., Gilfedder, B., et al. (2021). Transfer and transformations of oxygen in rivers as catchment reflectors of continental landscapes: a review. *Earth-Sci. Rev.* 220, 103729. doi: 10.1016/j.earscirev.2021.103729

Pierrot, D., Neill, C., Sullivan, K., Castle, R., Wanninkhof, R., Lüger, H., et al. (2009). Recommendations for autonomous underway pCO2 measuring systems and data-reduction routines. *Deep Sea Res. Part II.* 56, 512–522. doi: 10.1016/j.dsr2.2008.12.005

Planungsbüro U-Plan (2016). *Renaturierung des Haselbaches auf dem Gebiet der Stiftung Nantesbuch, Unterlagen zur wasserrechtlichen Genehmigung gemäß WPBV.* Unpublished Report.

Prijac, A., Gandois, L., Taillardat, P., Bourgault, M. A., Riahi, K., Ponçot, A., et al. (2023). Hydrological connectivity controls dissolved organic carbon exports in a peatland-dominated boreal catchment stream. *Hydrol. Earth Syst. Sci. Discuss.*, 2023, 1–33. doi: 10.5194/hess-2022-426

Pschenyckyj, C., Donahue, T., Kelly-Quinn, M., O'Driscoll, C., and Renou-Wilson, F. (2023). An examination of the influence of drained peatlands on regional stream water chemistry. *Hydrobiologia* 850, 3313–3339. doi: 10.1007/s10750-023-05188-5

Quick, A. M., Reeder, W. J., Farrell, T. B., Tonina, D., Feris, K. P., and Benner, S. G. (2019). Nitrous oxide from streams and rivers: a review of primary biogeochemical pathways and environmental variables. *Earth-Sci. Rev.* 191, 224–262. doi: 10.1016/j.earscirev.2019.02.021

Raymond, P. A., Caraco, N. F., and Cole, J. J. (1997). Carbon dioxide concentration and atmospheric flux in the Hudson River. *Estuaries* 20. 381–390. doi: 10.2307/1352351

Raymond, P. A., Hartmann, J., Lauerwald, R., Sobek, S., McDonald, C., Hoover, M., et al. (2013). Global carbon dioxide emissions from inland waters. *Nature* 503, 355–359. doi: 10.1038/nature12760

Raymond, P. A., Saiers, J. E., and Sobczak, W. V. (2016). Hydrological and biogeochemical controls on watershed dissolved organic matter transport: pulse-shunt concept. *Ecology* 97, 5–16. doi: 10.1890/14-1684.1

Raymond, P. A., Zappa, C. J., Butman, D., Bott, T. L., Potter, J., Mulholland, P., et al. (2012). Scaling the gas transfer velocity and hydraulic geometry in streams and small rivers. *Limnol. Oceanog.* 2, 41–53. doi: 10.1215/21573689-1597669

Rocher-Ros, G., Sponseller, R. A., Bergström, A.-K., Myrstener, M., and Giesler, R. (2020). Stream metabolism controls diel patterns and evasion of CO2 in Arctic streams. *Glob. Chang. Biol.* 26, 1400–1413. doi: 10.1111/gcb.14895

Sander, R. (2015). Compilation of Henry's law constants (version 4.0) for water as solvent. *Atmosph. Chem. Phys.* 15, 4399–4981. doi: 10.5194/acp-15-4399-2015

Sander, R., Acree, W. E., Visscher, A. D., Schwartz, S. E., and Wallington, T. J. (2022). Henry's law constants (IUPAC recommendations 2021). *Pure Appl. Chem.* 94, 71–85. doi: 10.1515/pac-2020-0302

Santos, I. R., Maher, D. T., and Eyre, B. D. (2012). Coupling Automated Radon and Carbon Dioxide Measurements in Coastal Waters. *Environ. Sci. Technol.* 46:7685–7691. doi: 10.1021/es301961b

Schneider, B., Sadkowiak, B., and Wachholz, F. (2007). A new method for continuous measurements of O2 in surface water in combination with pCO2 measurements: implications for gas phase equilibration. *Mar. Chem.* 103, 163–171. doi: 10.1016/j.marchem.2006.07.002

Smith, K. A., and Dobbie, K. E. (2001). The impact of sampling frequency and sampling times on chamber-based measurements of N2O emissions from fertilized soils. *Glob. Chang. Biol.* 7:933–945. doi: 10.1046/j.1354-1013.2001.00450.x

Song, C., Dodds, W. K., Rüegg, J., Argerich, A., Baker, C. L., Bowden, W. B., et al. (2018). Continental-scale decrease in net primary productivity in streams due to climate warming. *Nat. Geosci.* 11, 415–420. doi: 10.1038/s41561-018-0125-5

Stumm, W., and Morgan, J. J. (2012). *Aquatic Chemistry: Chemical Equilibria and Rates in Natural Waters.* Hoboken, NJ: John Wiley & Sons.

Taillardat, P., Bodmer, P., Deblois, C. P., Ponçot, A., Prijac, A., Riahi, K., et al. (2022). Carbon dioxide and methane dynamics in a peatland headwater stream: origins, processes and implications. *J. Geophys. Res.: Biogeosci.* 127, e2022JG006855. doi: 10.1029/2022JG006855

Tollefson, J., and Weiss, K. R. (2015). Nations approve historic global climate accord. *Nature* 528, 315–316. doi: 10.1038/528315a

Tseng, C.-Y., and Tinoco, R. O. (2020). A model to predict surface gas transfer rate in streams based on turbulence production by aquatic vegetation. *Adv. Water Resour.* 143, 103666. doi: 10.1016/j.advwatres.2020.103666

Upadhyay, P., Prajapati, S. K., and Kumar, A. (2023). Impacts of riverine pollution on greenhouse gas emissions: A comprehensive review. *Ecol. Indic.* 154, 110649. doi: 10.1016/j.ecolind.2023.110649

Vermaat, J., Hellmann, F., Dias, A., Hoorens, B., Logtestijn, R., and Aerts, R. (2011). Greenhouse gas fluxes from dutch peatland water bodies: importance of the surrounding landscape. *Wetlands* 31, 493–498. doi: 10.1007/s13157-011-0170-y

Wallin, M., Buffam, I., Öquist, M., Laudon, H., and Bishop, K. (2010). Temporal and spatial variability of dissolved inorganic carbon in a boreal stream network: Concentrations and downstream fluxes. *J. Geophys. Res.: Biogeosci.* 115, G02014. doi: 10.1029/2009JG001100

Wanninkhof, R., Asher, W. E., Ho, D. T., Sweeney, C., and McGillis, W. R. (2009). Advances in quantifying air-sea gas exchange and environmental forcing. *Ann. Rev. Mar. Sci.* 1, 213–244. doi: 10.1146/annurev.marine.010908.163742

Webb, J. R., Maher, D. T., and Santos, I. R. (2016). Automated, in situ measurements of dissolved CO2, CH4, and δ13C values using cavity enhanced laser absorption spectrometry: Comparing response times of air-water equilibrators. *Limnol. Oceanog.: Methods* 14, 323–337. doi: 10.1002/lom3.10092

Webb, J. R., Santos, I. R., Maher, D. T., and Finlay, K. (2019). The importance of aquatic carbon fluxes in net ecosystem carbon budgets: a catchment-scale review. *Ecosystems.* 22, 508–527. doi: 10.1007/s10021-018-0284-7

Zhang, W., Hu, Z., Audet, J., Davidson, T. A., Kang, E., Kang, X., et al. (2022). Effects of water table level and nitrogen deposition on methane and nitrous oxide emissions in an alpine peatland. *Biogeosciences* 19, 5187–5197. doi: 10.5194/bg-19-5187-2022